FATIGUE LIFETIME EVALUATION OF NOTCHED COMPONENTS: IMPLEMENTATION OF THE CONTROL VOLUME CONCEPT IN A STRAIN-BASED LCF CRITERION

Sabrina Vantadori, Andrea Carpinteri, Giovanni Fortese, Camilla Ronchei, Daniela Scorza, Andrea Zanichelli

Department of Engineering and Architecture, University of Parma, Parco Area delle Scienze 181/A 43124 Parma – Italy

Corresponding author:

Sabrina Vantadori, e-mail: sabrina.vantadori@unipr.it

Abstract

The goal of the present paper is to discuss the reliability of a strain-based multiaxial Low-Cycle Fatigue (LCF) criterion, recently proposed by some of the present authors, in estimating the fatigue lifetime of metallic structural components weakened by sharp notches. Such a criterion, based on the critical plane approach, is formulated according to the control volume concept related to the Strain Energy Density (SED) criterion: a material point located at a certain distance from the notch tip is assumed to be the verification point where to perform the fatigue assessment. The above distance is assumed to be a function of both the biaxiality ratio (applied shear stress amplitude over normal stress amplitude)

and the control volume radii under pure Mode I and pure Mode III loading conditions. Once the position of the verification point and the orientation of the critical plane are determined, the fatigue lifetime is theoretically evaluated through an equivalent normal strain amplitude acting on the critical plane, together with the tensile Manson-Coffin curve. Some uniaxial and multiaxial LCF data, recently published in the literature for V-notched round bars made of Ti-6Al-4V titanium alloy, are analysed through the present criterion.

NOMENCLATURE

e_1	notch geometry parameter related to Mode I
e_3	notch geometry parameter related to Mode III
I	error index
N_a	reference number of loading cycles to failure
$N_{f,cal}$	theoretical fatigue life
$N_{f,\exp}$	experimental fatigue life
P	verification point
$Puvw$	reference system attached to the critical plane
$Prtz$	fixed reference system
$P\hat{1}\hat{2}\hat{3}$	principal strain axes reference system at time instant for which the maximum principal strain, ε_1, attains its peak value over the loading cycle
r	distance of the verification point P from the notch tip
R_m	mean control volume radius
R_1	control volume radius related to Mode I
R_3	control volume radius related to Mode III
t	time
T_{RMS}	mean square error
$\boldsymbol{w}$	unit vector normal to the critical plane
α	phase angle between transversal normal strain ε_t and axial normal strain ε_z
α_{ur}, α_{ut}, α_{uz}	direction cosines of u-axis
α_{vr}, α_{vt}, α_{vz}	direction cosines of v-axis
α_{wr}, α_{wt}, α_{wz}	direction cosines of w-axis
β	phase angle between shear strain γ_{zt} and axial normal strain ε_z
γ_a	Manson-Coffin shear strain amplitude
γ_{zt}	shear strain
δ	angle between the averaged principal strain direction $\hat{1}$ and the normal $\boldsymbol{w}$ to the critical plane

3

ΔK_{1A}	Notch Stress Intensity Factor range under Mode I
ΔK_{3A}	Notch Stress Intensity Factor range under Mode III
$\Delta \sigma_{1A}$	High-Cycle Fatigue strength of smooth specimens under Mode I
$\Delta \tau_{3A}$	High-Cycle Fatigue strength of smooth specimens under Mode III
$\boldsymbol{\varepsilon}$	strain tensor at verification point P
$\varepsilon_{eq,a}$	equivalent normal strain amplitude
ε_a	Manson-Coffin normal strain amplitude
ε_r, ε_t	transversal normal strains
ε_z	axial normal strain
$\boldsymbol{\eta}_w$	displacement vector at verification point P, related to the critical plane
$\boldsymbol{\eta}_N$	normal displacement vector component of $\boldsymbol{\eta}_w$, related to the critical plane
$\boldsymbol{\eta}_C$	tangential displacement vector component of $\boldsymbol{\eta}_w$, related to the critical plane
κ	phase angle between transversal normal strain ε_r and axial normal strain ε_z
λ	biaxiality ratio, defined as the ratio between the applied shear stress amplitude and the normal stress amplitude
λ_1	eigenvalues for Mode I
λ_3	eigenvalues for Mode III
σ_a	applied normal stress amplitude
τ_a	applied shear stress amplitude
v	elastic Poisson ratio
v_{eff}	effective Poisson ratio
Φ	phase angle between tension and torsion loading
ω	pulsation

Subscripts

a	amplitude
m	mean value

1. INTRODUCTION

The state of the art clearly shows that the fatigue problem of mechanical components characterised by geometrical irregularities (such as notches, fillets and key-sets) has widely been examined in order to propose reliable methodologies for estimating the fatigue strength/lifetime under both uniaxial and multiaxial loadings [1-8].

Dealing with the fatigue failures of metallic structural components weakened by notches, the average Strain Energy Density (SED) criterion [9-12], originally proposed by Lazzarin and Zambardi [13], can be considered one of the most powerful engineering tool suitable for accurately performing the fatigue assessment of the above components.

Taking as starting point both the Neuber concept of an 'elementary material volume' [14,15] and the Sih criterion [16,17], Lazzarin and Zambardi adopted the average value of SED, evaluated over a control volume surrounding the notch tip, as a damage parameter for notched structural components. In particular, the radius of the control volume, over which the energy is averaged, was assumed to be a function of the notch geometry, the material fatigue limit evaluated on unnotched specimens, the threshold stress intensity factor range and the Poisson ratio. Moreover, according to such a criterion, fracture of brittle materials is expected to occur when the average value of SED is equal to a critical value, which is a material property [18].

The original version of the SED criterion [13] has been proposed for fatigue strength assessment of components weakened by sharp V-

notches subjected to tensile loading (Mode I), and blunt U and V-notches under Mode I loading have been examined in 2005 [19].

Subsequently, the SED criterion has been extended to notched components under mixed Mode loading [20-23]. Moreover, the aforementioned criterion has successfully been used also to perform the fatigue strength evaluation of both welded joints [24] and notched specimens under high-temperature conditions [25].

Then, an extension of the SED criterion to mechanical and structural components experiencing non-localised creep deformations has been proposed in 2016 [26]. Further, the criterion has recently been applied together with the Equivalent Material Concept (EMC) in order to estimate the failure loads of both U and V-notched aluminum plates characterised by large plastic deformations near the notch tip [27,28].

Note that the overall effectiveness of the above criterion when used to evaluate fatigue failures in notched metallic components has been analysed in Ref.[12]. In that paper, about one thousand experimental data taken from the literature for different materials and notches geometries have been examined, and a satisfactory agreement between experimental and theoretical results has been noticed.

In light of the efficiency and wide applicability of the SED criterion, some of the present authors have recently implemented the concept of the control volume in a strain-based criterion in order to estimate the fatigue life of severely notched specimens under Low-Cycle Fatigue (LCF) [29]. In particular, such a criterion, based on the critical plane approach, is a reformulation of its

6

counterpart for smooth metallic structural components [30,31] by considering the strain state at a material point P (named verification point in the following) located at a certain distance from the V-notch tip. Such a distance has been proposed to be directly linked to the control volume radius provided by the SED criterion. Then, the fatigue life evaluation is carried out at the verification point by employing an equivalent strain amplitude, related to the critical plane, together with a unique material reference curve (i.e. the tensile Manson-Coffin curve).

The aim of the present paper is to discuss the accuracy and reliability of the strain-based criterion together with the control volume concept (proposed in [29]) in estimating multiaxial LCF lifetime of structural components weakened by notches. Firstly, the analytical main points of such a criterion are outlined in Section 2. Then the fatigue experimental campaign reported in Refs [32,33] for V-notched round bars made of titanium grade 5 alloy (Ti-6Al-4V) is briefly summarised in Section 3. In Section 4, the criterion reported in Ref [29] is applied to the experimental fatigue data and, finally, some conclusions are provided in Section 5.

2. STRAIN-BASED CRITERION FORMULATION FOR SHARP V-NOTCHES

Now the analytical main points of the criterion proposed in Ref.[29] are briefly outlined.

The fatigue life assessment is carried out at point P (verification point), which is distant r from the V-notch tip (Fig. 1). More precisely, such a distance r, measured along the notch

7

bisector line, is assumed to depend on both the biaxiality ratio λ (defined as the ratio between the applied shear stress amplitude, τ_a, and the normal stress amplitude, σ_a) and the control volume radii under pure Mode I and pure Mode III [29]:

$$r = -(0.221)^{\lambda-1.484} \cdot R_m + 11.3 R_m \qquad (1)$$

where R_m is the mean control volume radius computed by averaging R_1 related to Mode I and R_3 related to Mode III, such control volume radii (R_1 and R_3) being provided by the SED criterion [20,21,32] through the following expressions:

$$R_1 = \left(\sqrt{2e_1} \cdot \frac{\Delta K_{1A}}{\Delta \sigma_{1A}} \right)^{\frac{1}{1-\lambda_1}} \qquad (2a)$$

$$R_3 = \left(\sqrt{\frac{e_3}{1+\nu}} \cdot \frac{\Delta K_{3A}}{\Delta \tau_{3A}} \right)^{\frac{1}{1-\lambda_3}} \qquad (2b)$$

e_1 and e_3 being two parameters depending on the V-notch geometry [32]. Further, ν is the elastic Poisson ratio, and λ_1 and λ_3 are the eigenvalues for Mode I and Mode III, respectively, calculated by means of a linear elastic finite element analysis as is reported in Ref. [32]. Moreover, ΔK_{1A} and ΔK_{3A} are the mean values of Mode I and Mode III Notch Stress Intensity Factors (NSIFs) ranges, respectively. Finally, the above control volume radii are also function of the High-Cycle Fatigue (HCF) strengths of smooth specimens ($\Delta \sigma_{1A}$ for Mode I, and $\Delta \tau_{3A}$ for Mode III), such strengths

being all referred to the same reference number N_a of loading cycles

to failure (for example, $N_a = 2 \cdot 10^6$).

Figure 1.

Once the position of the verification point P is determined

according to Eq. (1), the strain tensor at the above point is

obtained from a finite element analysis by examining a

tridimensional model.

If the structural component is subjected to synchronous out-of-

phase sinusoidal loadings, the strain state is characterised by two

transversal normal strains (ε_r and ε_t), one axial normal strain (ε_z)

and one shear strain (γ_{zt}):

$$\varepsilon_r = \varepsilon_{r,a} \; sin \; (\omega t - \kappa) + \varepsilon_{r,m} \tag{3a}$$

$$\varepsilon_t = \varepsilon_{t,a} \; sin \; (\omega t - \alpha) + \varepsilon_{t,m} \tag{3b}$$

$$\varepsilon_z = \varepsilon_{z,a} \; sin \; (\omega t) + \varepsilon_{z,m} \tag{3c}$$

$$\gamma_{zt} = \gamma_{zt,a} \; sin \; (\omega t - \beta) + \gamma_{zt,m} \tag{3d}$$

where ω = pulsation, t = time, κ, α, β = load phase angles. The

subscripts a and m refer to amplitude and mean value, respectively.

The strain tensor $\varepsilon(t)$ (at point P) with respect to the fixed

reference system $Prtz$ (Fig. 2(a)) is hence given by:

$$\mathbf{\varepsilon}(t) = \begin{bmatrix} \varepsilon_r(t) & 0 & 0 \\ 0 & \varepsilon_t(t) & \frac{1}{2}\gamma_{zt}(t) \\ 0 & \frac{1}{2}\gamma_{zt}(t) & \varepsilon_z(t) \end{bmatrix}$$

$$= \begin{bmatrix} \varepsilon_{r,a}\ sin(\omega t - \kappa) + \varepsilon_{r,m} & 0 & 0 \\ 0 & \varepsilon_{t,a}\ sin(\omega t - \alpha) + \varepsilon_{t,m} & \frac{1}{2}\gamma_{zt,a}\ sin(\omega t - \beta) + \frac{1}{2}\gamma_{zt,m} \\ 0 & \frac{1}{2}\gamma_{zt,a}\ sin(\omega t - \beta) + \frac{1}{2}\gamma_{zt,m} & \varepsilon_{z,a}\ sin(\omega t) + \varepsilon_{z,m} \end{bmatrix}$$

(4)

Figure 2.

Then, the critical plane orientation, which is linked to the averaged principal strain directions, has to be determined by using appropriate weight functions. In particular, the averaged directions of principal strain axes can be deduced on the basis of their instantaneous directions by means of the averaged principal Euler angles. By adopting the weight function $W(t)$ reported in Ref. [34], the averaged principal strain axes $\hat{1}, \hat{2}, \hat{3}$ coincide with the instantaneous ones at the time instant for which the maximum principal strain ε_1 (being $\varepsilon_1(t) \geq \varepsilon_2(t) \geq \varepsilon_3(t)$) attains its peak value over the loading cycle.

The orientation of the critical plane, which is the verification plane for fatigue life evaluation, is defined by taking an off-angle δ (in the principal averaged plane $\hat{1}\hat{3}$) formed by the normal $\mathbf{w}$ to the critical plane and the averaged direction $\hat{1}$. The off-angle δ is assumed to be expressed as follows:

$$\delta = \frac{3}{2}\left[1 - \left(\frac{1}{2(1+v_{eff})}\frac{\gamma_a}{\varepsilon_a}\right)^2\right]45° \qquad (5)$$

v_{eff} being the effective Poisson ratio. Moreover, ε_a and γ_a are determined by means of the tensile and torsional Manson-Coffin equations, respectively:

$$\varepsilon_a = \frac{\sigma'_f}{E}(2N_f)^b + \varepsilon'_f(2N_f)^c \qquad (6a)$$

$$\gamma_a = \frac{\tau'_f}{G}(2N_f)^{b_0} + \gamma'_f(2N_f)^{c_0} \qquad (6b)$$

where N_f is the number of loading cycles to failure, and σ'_f, ε'_f, b, c, τ'_f, γ'_f, b_0, c_0 are material constants, which can be deduced by running appropriate experimental tests. Note that Eq. (5) can be employed for metals ranging from ductile to extremely brittle fracture behaviour (details can be found in Refs [29-31]).

After defining the normal w to the critical plane, a local reference system $Puvw$ is taken into account, where the unit vector u is on the intersection line between the critical plane and the plane defined by the normal vector w and the z-axis; further, v is normal to u so that $Puvw$ forms a right-handed reference system (Fig. 2(b)). The directions cosines of the normal w can be computed with respect to the $Prtz$ as a function of two angles, φ and ϑ, in a spherical coordinate system ($0 \le \varphi < 2\pi$ and $0 \le \vartheta \le \pi$, Fig. 2(c)) [35]:

$$\alpha_{wr} = \sin\vartheta\cos\varphi, \qquad \alpha_{wt} = \sin\vartheta\sin\varphi, \qquad \alpha_{wz} = \cos\vartheta \qquad (7)$$

Furthermore, the direction cosines of the u- and v-axis are given by the following expressions [35]:

$$\alpha_{ur} = \cos\vartheta\cos\varphi, \qquad \alpha_{ut} = \cos\vartheta\sin\varphi, \qquad \alpha_{uz} = -\sin\vartheta \qquad (8a)$$

$$\alpha_{vr} = -\sin\varphi, \qquad \alpha_{vt} = \cos\varphi, \qquad \alpha_{vz} = 0 \qquad (8b)$$

Then, by taking into account the strain tensor $\varepsilon(t)$ at point P (Eq.(4)) with respect to the reference system $Puvw$, the displacement vector $\boldsymbol{\eta_w}$ related to the critical plane (Fig. 2(b)) can be expressed as follows:

$$\boldsymbol{\eta_w} = \boldsymbol{\varepsilon} \cdot \boldsymbol{w} \Rightarrow [\eta_w] = \begin{bmatrix} \varepsilon_r & 0 & 0 \\ 0 & \varepsilon_t & \frac{1}{2}\gamma_{zt} \\ 0 & \frac{1}{2}\gamma_{zt} & \varepsilon_z \end{bmatrix} \begin{bmatrix} \alpha_{wr} \\ \alpha_{wt} \\ \alpha_{wz} \end{bmatrix}$$

$$[\eta_w] = \begin{bmatrix} \eta_{w,r} \\ \eta_{w,t} \\ \eta_{w,z} \end{bmatrix} = \begin{bmatrix} \varepsilon_r \sin\vartheta\cos\varphi \\ \varepsilon_t \sin\vartheta\sin\varphi + \frac{1}{2}\gamma_{zt}\cos\vartheta \\ \frac{1}{2}\gamma_{zt}\sin\vartheta\sin\varphi + \varepsilon_z\cos\vartheta \end{bmatrix} \qquad (9)$$

and the scalar value $\eta_N(t)$ of the normal displacement vector $\boldsymbol{\eta_N}$ (Fig. 2(b)) is given by:

$$\eta_N(t) = (\boldsymbol{w} \cdot \boldsymbol{\eta_w}) \Rightarrow \eta_N(t) = \alpha_{wr}\eta_{w,r} + \alpha_{wt}\eta_{w,t} + \alpha_{wz}\eta_{w,z}$$
$$= \sin^2\vartheta\left[\varepsilon_r\cos^2\varphi + \varepsilon_t\sin^2\varphi\right] + \varepsilon_z\cos^2\vartheta + \gamma_{zt}\sin\varphi\sin\vartheta\cos\vartheta \qquad (10)$$

The mean value $\eta_{N,m}$ and the amplitude $\eta_{N,a}$ of $\eta_N(t)$ can be determined by substituting the strain components (Eqs (3)) into Eq. (10):

$$\eta_{N,m} = \sin^2\vartheta\left[\varepsilon_{r,m}\cos^2\varphi + \varepsilon_{t,m}\sin^2\varphi\right] + \varepsilon_{z,m}\cos^2\vartheta + \gamma_{zt,m}\sin\varphi\sin\vartheta\cos\vartheta \qquad (11a)$$

$$\eta_{N,a} = \sqrt{a^2 + b^2} \qquad (11b)$$

with:

$$a = \sin^2\vartheta\left[\varepsilon_{r,a}\cos\kappa\cos^2\varphi + \varepsilon_{t,a}\cos\alpha\sin^2\varphi\right] + \varepsilon_{z,a}\cos^2\vartheta + \gamma_{zt,a}\cos\beta\sin\varphi\sin\vartheta\cos\vartheta \qquad (12a)$$

$$b = -\sin^2\vartheta\left[\varepsilon_{r,a}\sin\kappa\cos^2\varphi + \varepsilon_{t,a}\sin\alpha\sin^2\varphi\right] - \gamma_{zt,a}\sin\beta\sin\varphi\sin\vartheta\cos\vartheta \qquad (12b)$$

Then, the normal displacement vector $\boldsymbol{\eta}_N$, perpendicular to the critical plane (Fig. 2(b)), is obtained from Eq. (10):

$$\boldsymbol{\eta}_N = (\boldsymbol{w}\cdot\boldsymbol{\eta}_w)\boldsymbol{w} \Rightarrow [\boldsymbol{\eta}_N] = \begin{bmatrix} \eta_{N,r} \\ \eta_{N,t} \\ \eta_{N,z} \end{bmatrix} \qquad (13)$$

where

$$\eta_{N,r} = \sin^3\vartheta\cos\varphi\left[\varepsilon_r\cos^2\varphi + \varepsilon_t\sin^2\varphi\right] + \sin\vartheta\cos\vartheta\cos\varphi\left[\varepsilon_z\cos\vartheta + \gamma_{zt}\sin\vartheta\sin\varphi\right] \qquad (14a)$$

$$\eta_{N,t} = \sin^3\vartheta\sin\varphi\left[\varepsilon_r\cos^2\varphi + \varepsilon_t\sin^2\varphi\right] + \sin\vartheta\cos\vartheta\sin\varphi\left[\varepsilon_z\cos\vartheta + \gamma_{zt}\sin\vartheta\sin\varphi\right] \qquad (14b)$$

$$\eta_{N,z} = \sin^2\vartheta\cos\vartheta\left[\varepsilon_r\cos^2\varphi + \varepsilon_t\sin^2\varphi\right] + \cos^2\vartheta\left[\varepsilon_z\cos\vartheta + \gamma_{zt}\sin\vartheta\sin\varphi\right] \qquad (14c)$$

By recalling Eqs (9) and (13), the tangential displacement vector $\boldsymbol{\eta}_C$ lying on the critical plane (Fig. 2(b)) can be computed according to the following expression:

$$\boldsymbol{\eta}_C = \boldsymbol{\eta}_w - \boldsymbol{\eta}_N \Rightarrow [\boldsymbol{\eta}_C] = \begin{bmatrix} \eta_{C,r} \\ \eta_{C,t} \\ \eta_{C,z} \end{bmatrix} \qquad (15)$$

where

$$\eta_{C,r} = \sin\vartheta\left[\cos\varphi\left(\varepsilon_r\cos^2\vartheta + (\varepsilon_r - \varepsilon_t)\sin^2\vartheta\sin^2\varphi - \varepsilon_z\cos^2\vartheta\right)\right] - \gamma_{zt}\sin^2\vartheta\cos\vartheta\sin\varphi\cos\varphi \qquad (16a)$$

$$\eta_{C,t} = \sin\vartheta\left[\sin\varphi\left(\varepsilon_t\cos^2\vartheta + (\varepsilon_t - \varepsilon_r)\sin^2\vartheta\sin^2\varphi - \varepsilon_z\cos^2\vartheta\right)\right] + \frac{1}{2}\gamma_{zt}\cos\vartheta\left(1 - 2\sin^2\vartheta\sin^2\varphi\right) \qquad (16b)$$

$$\eta_{C,z} = -\sin^2\vartheta\cos\vartheta\left[\varepsilon_r\cos^2\varphi + \varepsilon_t\sin^2\varphi - \varepsilon_z\right] + \frac{1}{2}\gamma_{zt}\sin\vartheta\sin\varphi\left(1 - 2\cos^2\vartheta\right) \qquad (16c)$$

Since the direction of vector $\boldsymbol{\eta}_C$ is generally time-varying, the mean value $\eta_{C,m}$ and the amplitude $\eta_{C,a}$ are not uniquely defined, and

13

different methods have been proposed in the literature (for instance, the Prismatic Hull method [36,37]). In the present paper, a min-max procedure to define $\eta_{C,m}$ and $\eta_{C,a}$ is applied [38] by examining the components of $\boldsymbol{\eta}_C$ along both u- and v-axis:

$$\eta_{C_u} = \boldsymbol{u} \cdot \boldsymbol{\eta}_C \Rightarrow \eta_{C_u} = \alpha_{ur}\eta_{C,r} + \alpha_{ut}\eta_{C,t} + \alpha_{uz}\eta_{C,z} \tag{17a}$$

$$\eta_{C_v} = \boldsymbol{v} \cdot \boldsymbol{\eta}_C \Rightarrow \eta_{C_v} = \alpha_{vr}\eta_{C,r} + \alpha_{vt}\eta_{C,t} + \alpha_{vz}\eta_{C,z} \tag{17b}$$

Recalling Eqs (3) and (16), the above expressions become:

$$\eta_{C_u} = f\, sin(\omega t) + g\, cos(\omega t) + \eta_{C_{u,m}} \tag{18a}$$

$$\eta_{C_v} = p\, sin(\omega t) + q\, cos(\omega t) + \eta_{C_{v,m}} \tag{18b}$$

where the mean values, $\eta_{C_{u,m}}$ and $\eta_{C_{v,m}}$, of the components of $\boldsymbol{\eta}_C$ along the u- and v-axis are given by:

$$\eta_{C_{u,m}} = \frac{1}{2} sin\, 2\vartheta \left[\varepsilon_{r,m}\, cos^2\, \varphi + \varepsilon_{t,m}\, sin^2\, \varphi - \varepsilon_{z,m} \right] + \frac{1}{2}\gamma_{zt,m}\, cos\, 2\vartheta\, sin\, \varphi \tag{19a}$$

$$\eta_{C_{v,m}} = sin\, \vartheta \left[\frac{1}{2}(\varepsilon_{t,m} - \varepsilon_{r,m}) sin\, 2\varphi \right] + \frac{1}{2}\gamma_{zt,m}\, cos\, \vartheta\, cos\, \varphi \tag{19b}$$

whereas the functions f, g, p, q are expressed by:

$$f = \frac{1}{2} sin\, 2\vartheta \left[\varepsilon_{r,a}\, cos\, \kappa\, cos^2\, \varphi + \varepsilon_{t,a}\, cos\, \alpha\, sin^2\, \varphi - \varepsilon_{z,a} \right] + \frac{1}{2}\gamma_{zt,a}\, cos\, \beta\, cos\, 2\vartheta\, sin\, \varphi \tag{20a}$$

$$g = -\frac{1}{2} sin\, 2\vartheta \left[\varepsilon_{r,a}\, sin\, \kappa\, cos^2\, \varphi + \varepsilon_{t,a}\, sin\, \alpha\, sin^2\, \varphi \right] - \frac{1}{2}\gamma_{zt,a}\, sin\, \beta\, cos\, 2\vartheta\, sin\, \varphi \tag{20b}$$

$$p = sin\, \vartheta \left[\frac{1}{2}(\varepsilon_{t,a}\, cos\, \alpha - \varepsilon_{r,a}\, cos\, \kappa) sin\, 2\varphi \right] + \frac{1}{2}\gamma_{zt,a}\, cos\, \beta\, cos\, \vartheta\, cos\, \varphi \tag{20c}$$

$$q = -sin\, \vartheta \left[\frac{1}{2}(\varepsilon_{t,a}\, sin\, \alpha - \varepsilon_{r,a}\, sin\, \kappa) sin\, 2\varphi \right] - \frac{1}{2}\gamma_{zt,a}\, sin\, \beta\, cos\, \vartheta\, cos\, \varphi \tag{20d}$$

Note that Eqs (18) are the parametric equations of the ellipse $\boldsymbol{s}$ described by the tip of the tangential displacement vector $\boldsymbol{\eta}_C$ on the critical plane during a loading cycle (Fig. 3). This ellipse is

centred at point $(\eta_{C_{u,m}} ; \eta_{C_{v,m}})$ and its semi-axes can be computed as follows:

$$\eta_{C,a} = \sqrt{\frac{f^2 + g^2 + p^2 + q^2}{2} + \sqrt{\left(\frac{f^2 + g^2 + p^2 + q^2}{2}\right)^2 (fq - gp)^2}} \qquad (21a)$$

$$\eta_{C,b} = \sqrt{\frac{f^2 + g^2 + p^2 + q^2}{2} - \sqrt{\left(\frac{f^2 + g^2 + p^2 + q^2}{2}\right)^2 (fq - gp)^2}} \qquad (21b)$$

The mean value $\eta_{C,m}$ of the tangential displacement component $\boldsymbol{\eta}_C$ on the critical plane is obtained from the following expression:

$$\eta_{C,m} = \sqrt{\eta_{C_{u,m}}^2 + \eta_{C_{v,m}}^2} \qquad (22)$$

whereas the amplitude of vector $\boldsymbol{\eta}_C$ coincides with the major semi-axis $\eta_{C,a}$ of the above ellipse.

Figure 3.

Then, the fatigue strength is assessed by means of an equivalent strain amplitude, $\varepsilon_{eq,a}$, together with a unique material reference curve (i.e. the tensile Manson-Coffin curve, Eq. (6a)). More precisely, the above equivalent strain amplitude is expressed by quadratically combining the amplitudes of both the normal ($\eta_{N,a}$, Eq (11b)) and the tangential ($\eta_{C,a}$, Eq. (21a)) displacement vectors acting on the critical plane:

$$\varepsilon_{eq,a} = \sqrt{(\eta_{N,a})^2 + \left(\frac{\varepsilon_a}{\gamma_a}\right)^2 (\eta_{C,a})^2} \qquad (23)$$

15

By equating Eq. (23) with Eq. (6a), the number N_f of loading cycles to failure can be worked out through an iterative procedure.

3. FATIGUE EXPERIMENTAL CAMPAIGN

The strain-based multiaxial LCF criterion formulated in conjunction with the control volume concept is applied to a set of data recently published in the literature [32,33]. Uniaxial and multiaxial fatigue tests on circumferentially V-notched round bars made of Ti-6Al-4V titanium alloy are briefly described in the present Section.

Each specimen presents a V-notch with depth equal to 6 mm, opening angle equal to $90°$ and notch root radius equal to about 0.1 mm. All specimens have been polished in order to remove surface scratches before performing the tests.

The experimental uniaxial and multiaxial fatigue tests have been carried out by means of a MTS 809 servo-hydraulic biaxial machine. All tests have been conducted under load control at a frequency value from 5 to 10 Hz, depending on the applied load. Details of the loading conditions being examined are reported in Tables 1-3, where $N_{f,exp}$ is the experimental fatigue life.

Table 1.

Table 2.

Table 3.

According to the notch geometry and the material properties (that is, the values of the elastic Poisson ratio, the eigenvalues of Mode I and Mode III, the NSIFs ranges, and the HCF strengths) reported in the original papers [32,33], the control volume radius R_1 is equal to 0.051 mm (Eq. (2a)), whereas the control volume radius R_3 is equal to 0.837 mm (Eq. (2b)). The above difference in the values of control volume radii is not only due to the different behaviour in the crack propagation process under either tension or torsion loading, but also to the higher plasticity around the notch tip experienced under torsion with respect to that under tension.

4. CRITERION VALIDATION AND DISCUSSION

The present strain-based multiaxial LCF criterion is here applied to the experimental data described in the previous Section.

All experimental data being examined are characterised by a fatigue life between 10^3 and $6 \cdot 10^5$ loading cycles and a nominal load ratio equal to -1. Six different fatigue test series on V-notched specimens are here analysed (Tables 1-3):

(1) two series of tests under pure tension (specimens No. 1-6 in Table 1) and pure torsion (specimens No. 7-11 in Table 1) fatigue loading;

(2) two series of tests under combined in- ($\Phi = 0°$) and out-of-phase ($\Phi = 90°$) tension and torsion loading, with constant biaxiality ratio λ equal to 0.6 (Table 2);

(3) two series of tests under combined in- ($\Phi=0°$) and out-of-phase ($\Phi=90°$) tension and torsion loading, with constant biaxiality ratio λ equal to 2.0 (Table 3).

Different values of the distance r to determine the verification point position are computed according to Eq. (1):

(a) for pure tension loading (that is, $\lambda=0$), r is equal to $1.9 \cdot R_m$;

(b) for pure torsion loading (that is, $\lambda=\infty$), r is equal to $11.3 \cdot R_m$;

(c) for combined in- and out-of-phase tension and torsion loading characterised by $\lambda=0.6$, r is equal to $7.5 \cdot R_m$;

(d) for combined in- and out-of-phase tension and torsion loading characterised by $\lambda=2.0$, r is equal to $10.8 \cdot R_m$.

Note that Eq. (1) has been obtained from a best-fit procedure by considering some values of λ related to the experimental data reported in Ref. [32,33]. In particular, the following error index, I, has been optimised in order to determine the data-points to be interpolated:

$$I = \frac{\sqrt{\left(\eta_{N,a}\right)^2 + \left(\dfrac{\varepsilon_a}{\gamma_a}\right)^2 \left(\eta_{C,a}\right)^2} - \varepsilon_a}{\varepsilon_a} \tag{24}$$

where ε_a and γ_a are defined by means of Eqs (6a) and (6b), respectively.

As is previously discussed, in order to estimate the fatigue lifetime of the V-notched specimens, the strain tensor at the verification point P has been estimated from a finite element analysis by means of the commercial software Straus7® [39]. More precisely, the strain state at the verification point, for every

investigated fatigue test, has been determined through a tridimensional model by using both 6- and 8-node finite elements. Taking advantage of the geometric symmetry, only one-half of the specimen has been modelled, as is shown in Figure 4. Furthermore, the mesh size has been gradually refined nearing the region containing the notch tip (Fig. 4(b)). The results in terms of strains have been determined by running a series of linear transient dynamic analyses in order to simulate the experimental tests performed by Berto et al. [32,33].

Figure 4.

The Von Mises stress distribution for combined in-phase tension and torsion loading characterised by $\lambda = 2.0$ and $\Phi = 0°$ is shown in **Figure 5,** at the time instant corresponding to the maximum value of the both normal and shear stresses applied.

Figure 5.

The values of the material parameters of the Manson-Coffin curves, required for applying the strain-based criterion, are reported in Ref. [29]. The effective Poisson ratio, ν_{eff}, is assumed to be equal to the elastic Poisson ratio (that is, $\nu = 0.3$).

Once the strain state at point P is numerically determined and the above material parameters are deduced, the fatigue lifetime can be estimated by using the present strain-based multiaxial LCF criterion together with the control volume concept.

The comparison between experimental, $N_{f,exp}$, and theoretical, $N_{f,cal}$, evaluation in terms of fatigue life for both uniaxial and multiaxial loadings is shown in Figs 6(a) and 6(b), respectively. Note that the solid line indicates $N_{f,cal} = N_{f,exp}$, whereas the dash-dot lines correspond to $N_{f,cal}/N_{f,exp}$ equal to 0.3 and 3.0. This comparison clearly proves that:

- for uniaxial fatigue loading (that is, pure tension and pure torsion loading, Fig. 6(a)), 71% of fatigue life calculations are included into 3x band;

- for multiaxial fatigue loading (that is, combined tension and torsion loading with $\lambda = 0.6$ and 2.0, Fig. 6(b)), 76% of fatigue life calculations are included into 3x band. Note that better results are obtained for multiaxial fatigue data characterised by biaxiality ratio equal to 0.6. That is due to the fact that the relationship between r and λ (Eq. (1)) has been deduced by taking into account only the experimental data with $\lambda = 0.6$ and not those with λ equal to 2.0.

Figure 6.

The accuracy of the present fatigue lifetime estimation can also be evaluated by means of the root mean square error method [40]. In more detail, the value of the root mean square logarithmic error is computed as follows:

$$E_{RMS} = \sqrt{\frac{\sum_{i=1}^{j} log^2\left(N_{f,exp}/N_{f,cal}\right)_i}{j}} \qquad (25)$$

where j is the total number of data, and the mean square error T_{RMS} is given by:

$$T_{RMS} = 10^{E_{RMS}} \qquad (26)$$

If all the computed results fell, for instance, within the 3x band, the value of T_{RMS} would be equal to 3.

Figure 7 shows the mean square error computed for all values of fatigue life, in accordance with the different fatigue test series previously presented.

Figure 7.

The analysis of the results in terms of the mean square error indicates that the agreement between experimental and theoretical fatigue lives is satisfactory, the value of the T_{RMS} being lower than 3, and that holds true for all the loading conditions being examined.

On the basis of such encouraging results, we can remark that the joined application of the strain-based criterion together with the concept of the control volume radii (provided by the SED criterion) seems to be a promising engineering tool, able to perform the fatigue lifetime evaluation with an adequate accuracy.

5. CONCLUSIONS

In the present paper, the multiaxial fatigue life assessment of components weakened by sharp notches has been performed by employing a strain-based multiaxial LCF criterion in conjunction with the concept of control volume radius, related to the SED criterion originally proposed by Lazzarin and co-workers. In particular, such a radius has been assumed to be a function of both the notch geometry and the material properties.

According to the present criterion, the fatigue assessment has been carried out at a verification point, which is located at a certain distance from the notch tip, depending such a distance on both the biaxiality ratio and the control volume radii under loading conditions of pure Mode I and pure Mode III.

Once the position of the verification point and the orientation of the critical plane have been determined, the fatigue lifetime has theoretically been evaluated through an equivalent normal strain amplitude, acting on the critical plane, together with the tensile Manson-Coffin curve.

Some uniaxial and multiaxial fatigue data, recently published in the literature, have been analysed to evaluate the effectiveness of the present criterion. The agreement between experimental data and theoretical fatigue lives is satisfactory.

Therefore, the present criterion seems to be a promising tool to assess the fatigue lifetime of notched structural components, although both more complex loading configurations (characterised by nominal load ratio different from -1) and different notch geometries

(i.e. blunt notches) need to be processed in order to devise a robust procedure suitable for practical applications.

REFERENCES

[1] E. Castillo, A. Fernandez-Canteli, A general regression model for lifetime evaluation and prediction, Int. J. Fracture 107 (2001) 117-137.

[2] E. Castillo, A. Fernandez-Canteli, H. Pinto, M. Lopez-Aenlle, A general regression model for statistical analysis of strain-life data, Materials Letters D 62 (2008) 3639-3642.

[3] A.M.P De Jesus, J.A.F.O. Correia, Critical assessment of a local strain-based fatigue crack growth model using experimental data available for the P355NL1 steel, Journal of Pressure Vessel Technology. 135 (2013) Article number 11404.

[4] N. Gates, A. Fatemi, Notch deformation and stress gradient effects in multiaxial fatigue, Theor. Appl. Fract. Mech. 84 (2016) 3-25.

[5] A. Ince, Numerical validation of computational stress and strain analysis model for notched components subject to non-proportional loadings, Theor. Appl. Fract. Mech. 84 (2016) 26-37.

[6] M.A. Meggiolaro, J.T.P. Castro, R.C. de Oliveira Góes, Elastoplastic nominal stress effects in the estimation of the notch-tip behavior in tension, Theor. Appl. Fract. Mech. 84 (2016) 86-92.

[7] V. Chaves, C. Madrigal, A. Navarro, Fatigue limit predictions at stress concentrations using FEA and microstructural fracture mechanics, Theor. Appl. Fract. Mech. 87 (2017) 11-20.

[8] P. Gallo, S. Bressan, T. Morishita, T. Itoh, F. Berto, Analysis of multiaxial low cycle fatigue of notched specimens for type 316L stainless steel under non-proportional loading, Theor. Appl. Fract. Mech. 89 (2017) 79-89.

[9] F. Berto, P. Lazzarin, A review of the volume-based strain energy density approach applied to V-notches and welded structures, Theor. Appl. Fract. Mech. 52 (2009) 183-194.

[10] P. Lazzarin, A. Campagnolo, F. Berto, A comparison among some recent energy- and stress-based criteria for the fracture assessment of sharp V-notched components under Mode I loading, Theor. Appl. Fract. Mech. 71 (2014) 21-30.

[11] D. Radaj, State-of-the-art review on the local strain energy density concept and its relation to the J-integral and peak stress method, Fatigue Fract. Eng. Mater. Struct. 38 (2015) 2-28.

[12] F. Berto, Fatigue and fracture assessment of notched components by means of the Strain Energy Density, Eng. Fract. Mech. 167 (2016) 176-187.

[13] P. Lazzarin, R. Zambardi, A finite-volume-energy based approach to predict the static and fatigue behavior of components with sharp V-shaped notches, Int. J. Fract. 112 (2001) 275-298.

[14] H. Neuber, Theory of Notch Stresses, Springer-Verlag, Berlin, 1958.

[15] H. Neuber, Uber die Berücksichtigung der Spannungskonzentration bei Festigkeitsberechnungen, Konstruktion 20 (1968) 245-251.

[16] G.C. Sih, Strain-energy-density factor applied to mixed mode crack problems, Int. J. Fract. 10 (1974) 305-321.

[17] G.C. Sih, J.W. Ho, Sharp notch fracture strength characterized by critical energy density, Theor. Appl. Fract. Mech. 16 (1991) 179-214.

[18] E. Beltrami, Sulle condizioni di resistenza dei corpi elastici, Il Nuovo Cimento 18 (1885) (in Italian).

[19] P. Lazzarin, F. Berto, Some expressions for the strain energy in a finite volume surrounding the root of blunt V-notches. Int. J. Fract. 135 (2005) 161-185.

[20] B. Atzori, F. Berto, P. Lazzarin, M. Quaresimin, Multi-axial fatigue behaviour of a severely notched carbon steel, Int. J. Fatigue 28 (2006) 485-493.

[21] F. Berto, P. Lazzarin, R. Tovo, Multiaxial fatigue strength of severely notched cast iron specimens, Int. J. Fatigue 67 (2014) 15-27.

[22] G. Meneghetti, A. Campagnolo, F. Berto, B. Atzori, Averaged strain energy density evaluated rapidly from the singular peak stresses by FEM: cracked components under mixed-mode (I+II) loading, Theor. Appl. Fract. Mech. 79 (2015) 113-124.

[23] F. Berto, M.R. Ayatollahi, T. Borsato, P. Ferro, Local strain energy density to predict size-dependent brittle fracture of cracked specimens under mixed mode loading, Theor. Appl. Fract. Mech. 86(part B) (2016) 217-224.

[24] P. Lazzarin, F. Berto, B. Atzori, A synthesis of data from steel spot welded joints of reduced thickness by means of local SED, Theor. Appl. Fract. Mech. 63-64 (2013) 32-39.

[25] P. Gallo, F. Berto, P. Lazzarin, High temperature fatigue tests of notched specimens made of titanium Grade 2, Theor. Appl. Fract. Mech. 76 (2015) 27-34.

[26] P. Gallo, F. Berto, G. Glinka, Analysis of creep stresses and strains around sharp and blunt V-notches, Theor. Appl. Fract. Mech. 85(part B) (2016) 435-446.

[27] A.R. Torabi, F. Berto, A. Campagnolo, J. Akbardoost, Averaged strain energy density criterion to predict ductile failure of U-notched Al 6061-T6 plates under mixed mode loading, Theor. Appl. Fract. Mech. ISSN: 0167-8442, doi: 10.1016/j.tafmec.2017.04.010 (in press).

[28] A.R. Torabi, F. Berto, S.M.J. Razavi, Ductile failure prediction of thin notched aluminum plates subjected to combined tension-shear loading, Theor. Appl. Fract. Mech. ISSN: 0167-8442, doi: 10.1016/j.tafmec.2017.05.003 (in press).

[29] A. Carpinteri, F. Berto, A. Campagnolo, G. Fortese, C. Ronchei, D. Scorza, S. Vantadori, Fatigue assessment of notched specimens by means of a critical plane-based criterion and energy concepts, Theor. Appl. Fract. Mech. 84 (2016) 57-63.

[30] A. Carpinteri, C. Ronchei, A. Spagnoli, S. Vantadori, Lifetime estimation in the low/medium-cycle regime using the Carpinteri–Spagnoli multiaxial fatigue criterion, Theor. Appl. Fract. Mech. 73 (2014) 120–127.

[31] A. Carpinteri, C. Ronchei, D. Scorza, S. Vantadori, Fatigue life estimation for multiaxial low-cycle fatigue regime: the influence of the effective Poisson ratio value, Theor. Appl. Fract. Mech. 79 (2015) 77–83.

[32] F. Berto, A. Campagnolo, P. Lazzarin, Fatigue strength of severely notched specimens made of Ti-6Al-4V under multiaxial loading, Fatigue Fract. Eng. Mater. Struct. 38 (2015) 503–517.

[33] F. Berto, A. Campagnolo, T. Welo, Local strain energy density to assess the multiaxial fatigue strength of titanium alloys, Frattura ed Integrità Strutturale 10 (2016) 69-79.

[34] A. Carpinteri, A. Spagnoli, S. Vantadori, C. Bagni, Structural integrity assessment of metallic components under multiaxial fatigue: the C-S criterion and its evolution. Fatigue Fract. Eng. Mater. Struct. 36 (2013) 870-883.

[35] A. Carpinteri, A. Spagnoli, Multiaxial high-cycle fatigue criterion for hard metals, Int. J. Fatigue 23 (2001) 135–145.

[36] J.A. Araújo, A. Carpinteri, C. Ronchei, A. Spagnoli, S. Vantadori, An alternative definition of the shear stress amplitude based on the Maximum Rectangular Hull method and application to the C–S (Carpinteri–Spagnoli) criterion, Fatigue Fract. Eng. Mater. Struct. 37 (2014) 764–771.

[37] A. Carpinteri, C. Ronchei, A. Spagnoli, S. Vantadori, On the use of the Prismatic Hull method in a critical plane-based multiaxial fatigue criterion, Int. J. Fatigue 68 (2014) 159–167.

[38] I. Papadopoulos, Critical plane approaches in high-cycle fatigue: on the definition of the amplitude and mean value of the shear stress acting on the critical plane, Fatigue Fract. Eng. Mater. Struct. 21 (1998) 269-285.

[39] Straus7, Theoretical Manual: Theoretical Background for Straus7 Finite Element Analysis Systems, G+D Computing, Sydney, 2004.

[40] T. Łagoda, K. Walat, Lifetime of semi-ductile materials through the critical plane approach, Int. J. Fatigue 67 (2014) 73-77.

FATIGUE LIFETIME EVALUATION OF NOTCHED COMPONENTS: IMPLEMENTATION OF THE CONTROL VOLUME CONCEPT IN A STRAIN-BASED LCF CRITERION

Sabrina Vantadori, Andrea Carpinteri, Giovanni Fortese,

Camilla Ronchei, Daniela Scorza, Andrea Zanichelli

Department of Engineering and Architecture,

University of Parma, Parco Area delle Scienze 181/A

43124 Parma – Italy

Corresponding author:

Sabrina Vantadori, e-mail: sabrina.vantadori@unipr.it

LIST OF FIGURES AND TABLES CAPTIONS

Figure 1. Position of the verification point P according to the volume radii R_1 and R_3 for sharp notch.

Figure 2. (a) *Prtz* fixed reference system; (b) *Puvw* reference system and displacement components related to the critical plane; (c) angles φ and ϑ in the spherical coordinate system.

Figure 3. Ellipse **s** described by the tip of the tangential displacement vector $\boldsymbol{\eta}_C$ on the critical plane during a loading cycle.

Table 1. Uniaxial loading conditions of the experimental tests being examined.

Table 2. Multiaxial loading conditions (with biaxiality ratio λ equal to 0.6) of the experimental tests being examined.

Table 3. Multiaxial loading conditions (with biaxiality ratio λ equal to 2.0) of the experimental tests being examined.

Figure 4. Tridimensional finite element model of the V-notched specimen: (a) prospective view; (b) detailed view in the close neighbourhood of the notch.

Figure 5. The Von Mises stress distribution for combined in-phase tension and torsion loading characterised by $\lambda = 2.0$ and $\Phi = 0°$, at the time instant corresponding to the maximum value of the both normal and shear stresses applied.

Figure 6. Comparison between theoretical and experimental fatigue life: (a) uniaxial loading; (b) multiaxial loading.

Figure 7. Mean square error determined by applying the strain-based criterion together with the control volume concept, for different loading conditions.
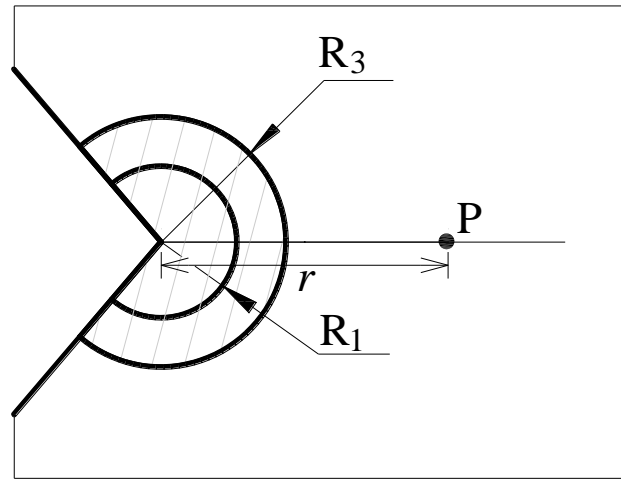
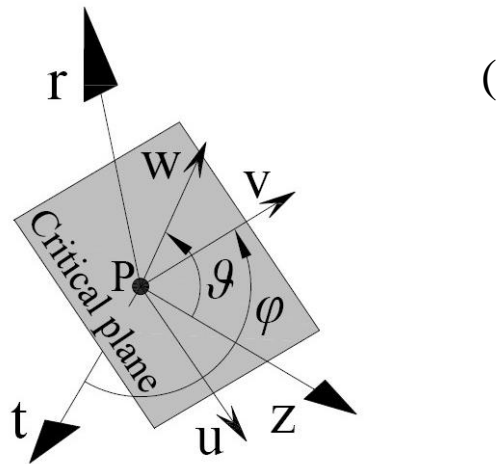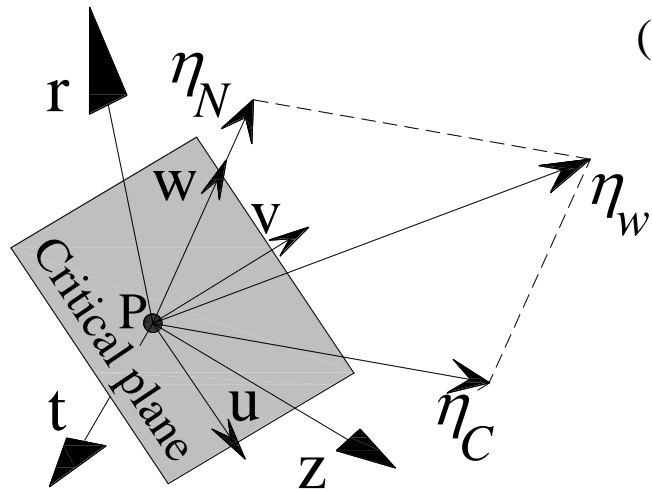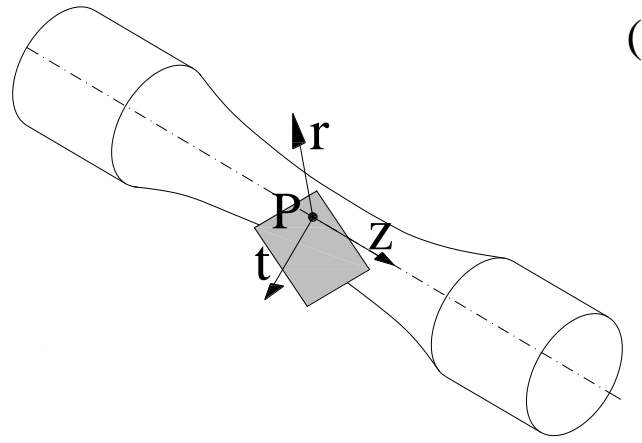**Figure 1.** Position of the verification point P according to the volume radii R_1 and R_3 for sharp notch.

Figure 2. (a) *Prtz* fixed reference system; (b) *Puvw* reference system and displacement components related to the critical plane; (c) angles φ and ϑ in the spherical coordinate system.
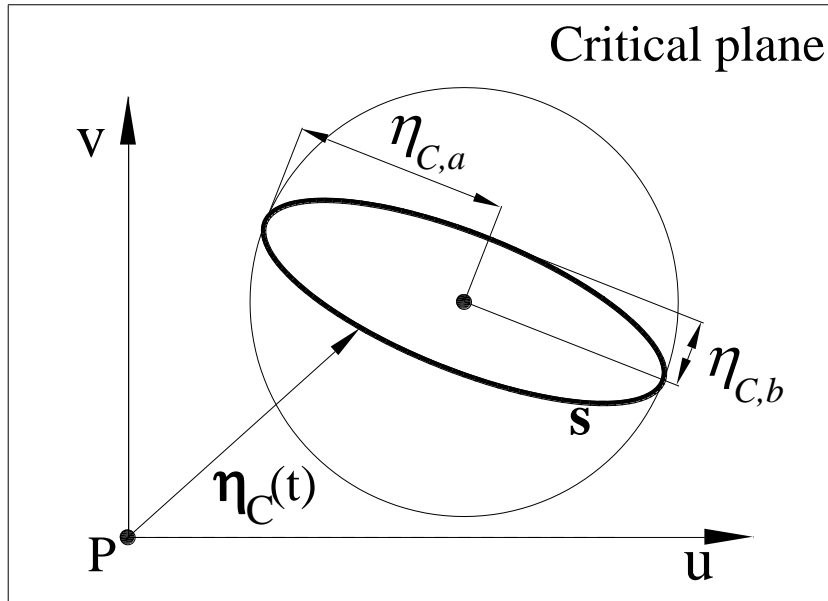
Figure 3. Ellipse **s** described by the tip of the tangential displacement vector $\boldsymbol{\eta}_C$ on the critical plane during a loading cycle.

Table 1. Uniaxial loading conditions of the experimental tests being examined.

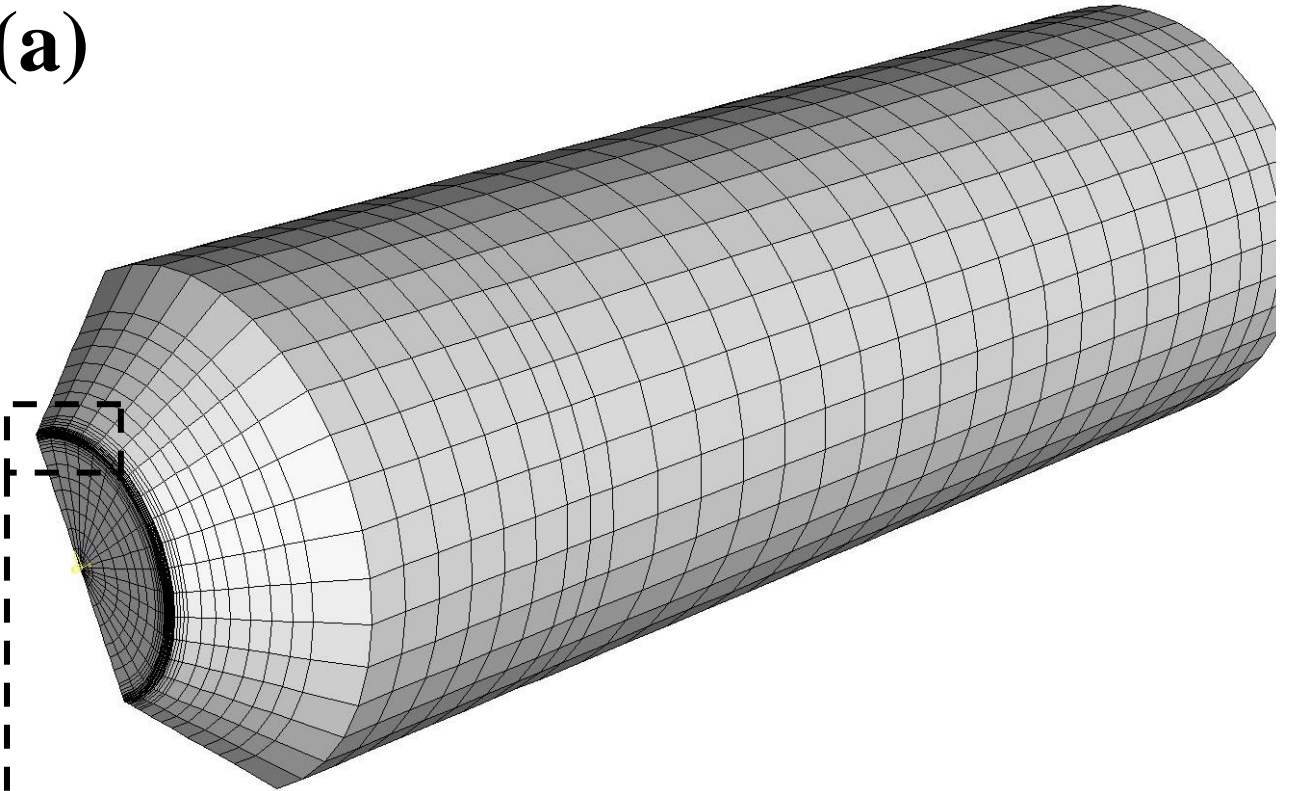| Material	No.	Φ [°]	λ	σ_a [MPa]	τ_a [MPa]	$N_{f,exp}$ [cycles]
Ti-6Al-4V Titanium Alloy	1	0	0	160.0	-	99067
	2	0	0	160.0	-	107540
	3	0	0	200.0	-	24772
	4	0	0	200.0	-	33670
	5	0	0	230.0	-	11164
	6	0	0	230.0	-	13456
	7	0	∞	-	380.0	46496
	8	0	∞	-	380.0	65569
	9	0	∞	-	400.0	19520
	10	0	∞	-	420.0	7518
	11	0	∞	-	460.0	1053

Table 2. Multiaxial loading conditions (with biaxiality ratio λ equal to 0.6) of the experimental tests being examined.

Material	No.	Φ [°]	λ	σ_a [MPa]	τ_a [MPa]	$N_{f,exp}$ [cycles]
	1	0	0.6	130.0	78.0	137540
	2	0	0.6	140.0	84.0	93785
	3	0	0.6	140.0	84.0	141768
	4	0	0.6	160.0	96.0	67500
	5	0	0.6	160.0	96.0	85000
	6	0	0.6	170.0	102.0	36177
	7	0	0.6	170.0	102.0	43400
Ti-6Al-4V	8	0	0.6	190.0	114.0	12668
Titanium Alloy	9	0	0.6	190.0	114.0	15346
	10	90	0.6	130.0	78.0	182284
	11	90	0.6	130.0	78.0	237488
	12	90	0.6	140.0	84.0	74178
	13	90	0.6	140.0	84.0	91230
	14	90	0.6	170.0	102.0	19789
	15	90	0.6	170.0	102.0	26540
	16	90	0.6	190.0	114.0	10698

Table 3. Multiaxial loading conditions (with biaxiality ratio λ equal to 2.0) of the experimental tests being examined.

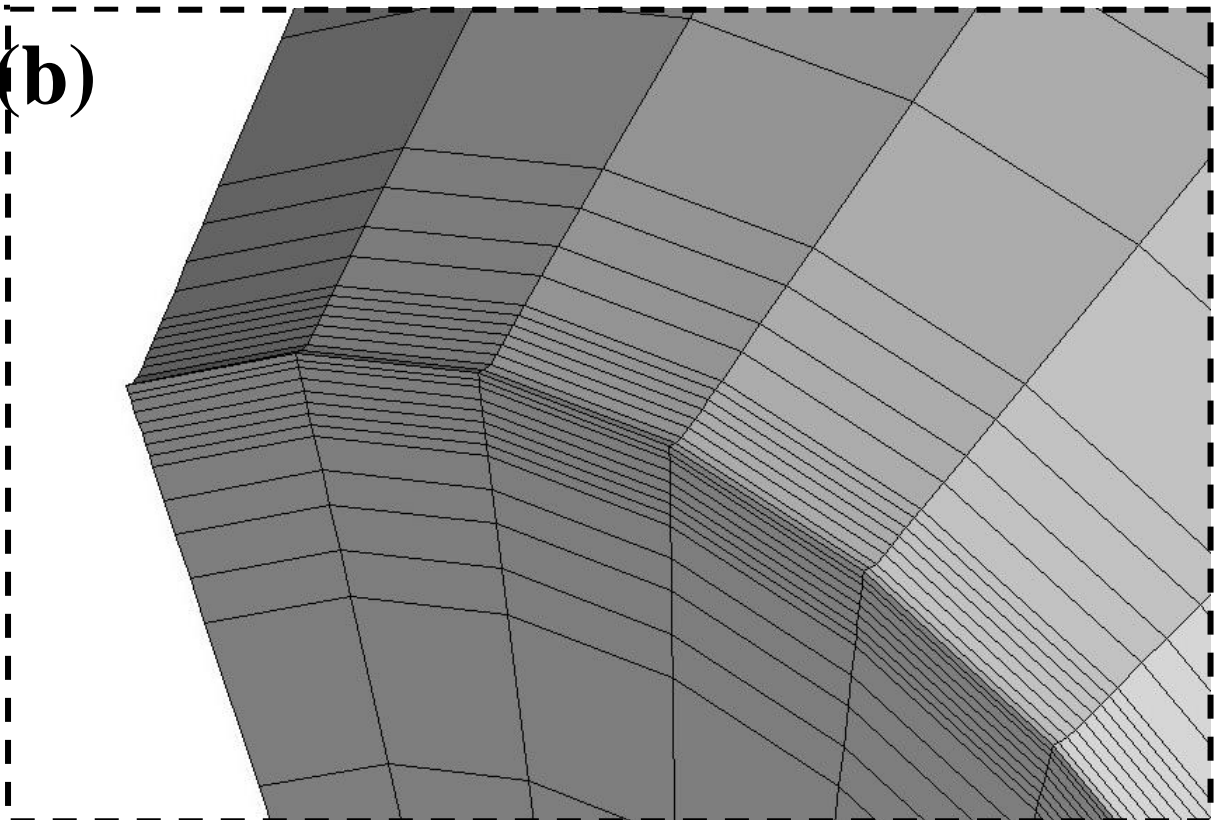| Material	No.	Φ [°]	λ	σ_a [MPa]	τ_a [MPa]	$N_{f,exp}$ [cycles]
	1	0	2.0	90	180	384500
	2	0	2.0	90	180	390000
	3	0	2.0	90	180	455000
	4	0	2.0	90	180	567300
	5	0	2.0	90	180	622000
	6	0	2.0	90	180	750000
	7	0	2.0	90	180	834000
	8	0	2.0	100	200	198000
	9	0	2.0	100	200	206000
	10	0	2.0	100	200	221000
	11	0	2.0	110	220	103000
	12	0	2.0	110	220	108475
	13	0	2.0	110	220	112000
	14	0	2.0	110	220	121000
	15	0	2.0	130	260	27500
	16	0	2.0	130	260	34500
	17	0	2.0	130	260	38000
	18	0	2.0	130	260	54021
Ti-6Al-4V	19	0	2.0	140	280	16500
Titanium Alloy	20	0	2.0	140	280	19000
	21	0	2.0	150	300	10200
	22	0	2.0	150	300	12000
	23	0	2.0	150	300	13400
	24	90	2.0	100	200	506280
	25	90	2.0	100	200	621000
	26	90	2.0	110	220	182000
	27	90	2.0	110	220	225000
	28	90	2.0	110	220	301000
	29	90	2.0	120	240	131200
	30	90	2.0	120	240	154000
	31	90	2.0	130	260	87500
	32	90	2.0	130	260	96000
	33	90	2.0	130	260	118500
	34	90	2.0	150	300	18900
	35	90	2.0	150	300	22000
	36	90	2.0	150	300	26500
	37	90	2.0	150	300	31500
	38	90	2.0	170	340	8900
	39	90	2.0	170	340	11000

(a)

(b)

Figure 4. Tridimensional finite element model of the V-notched specimen: (a) prospective view; (b) detailed view in the close neighbourhood of the notch.
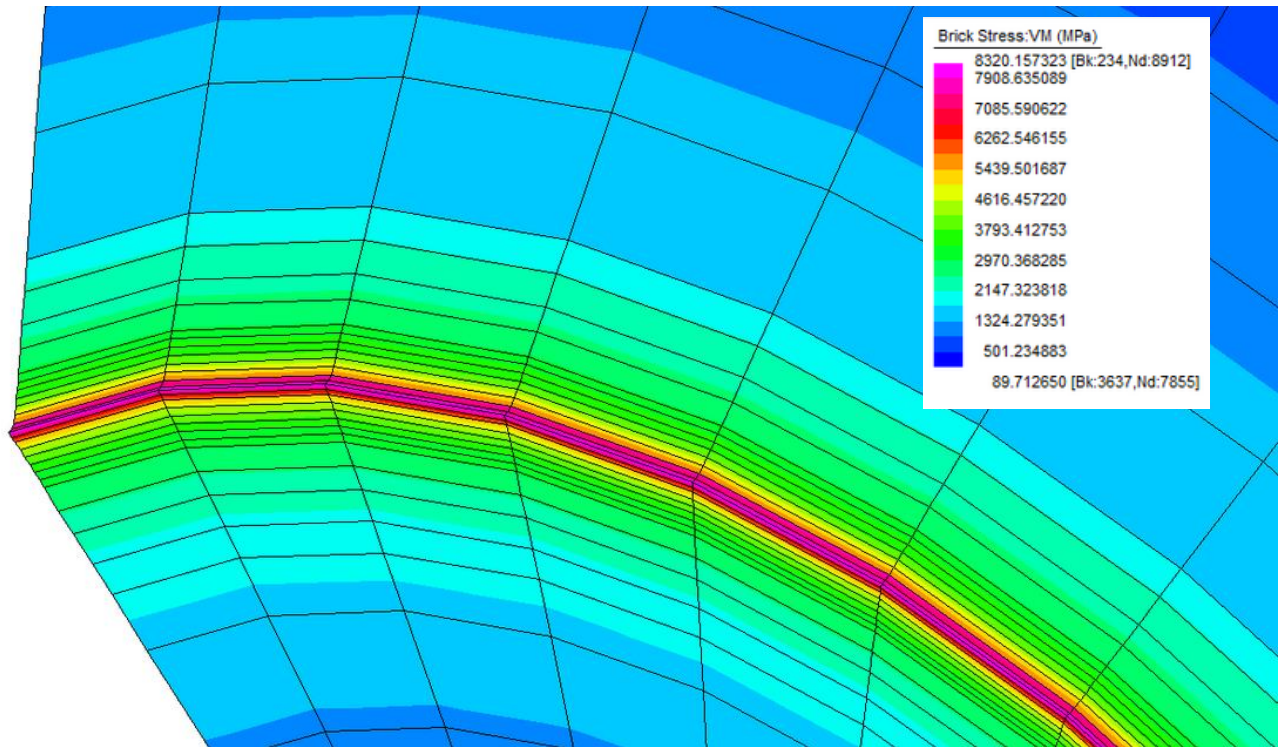
Figure 5. The Von Mises stress distribution for combined in-phase tension and torsion loading characterised by $\lambda = 2.0$ and $\Phi = 0°$, at the time instant corresponding to the maximum value of the both normal and shear stresses applied.
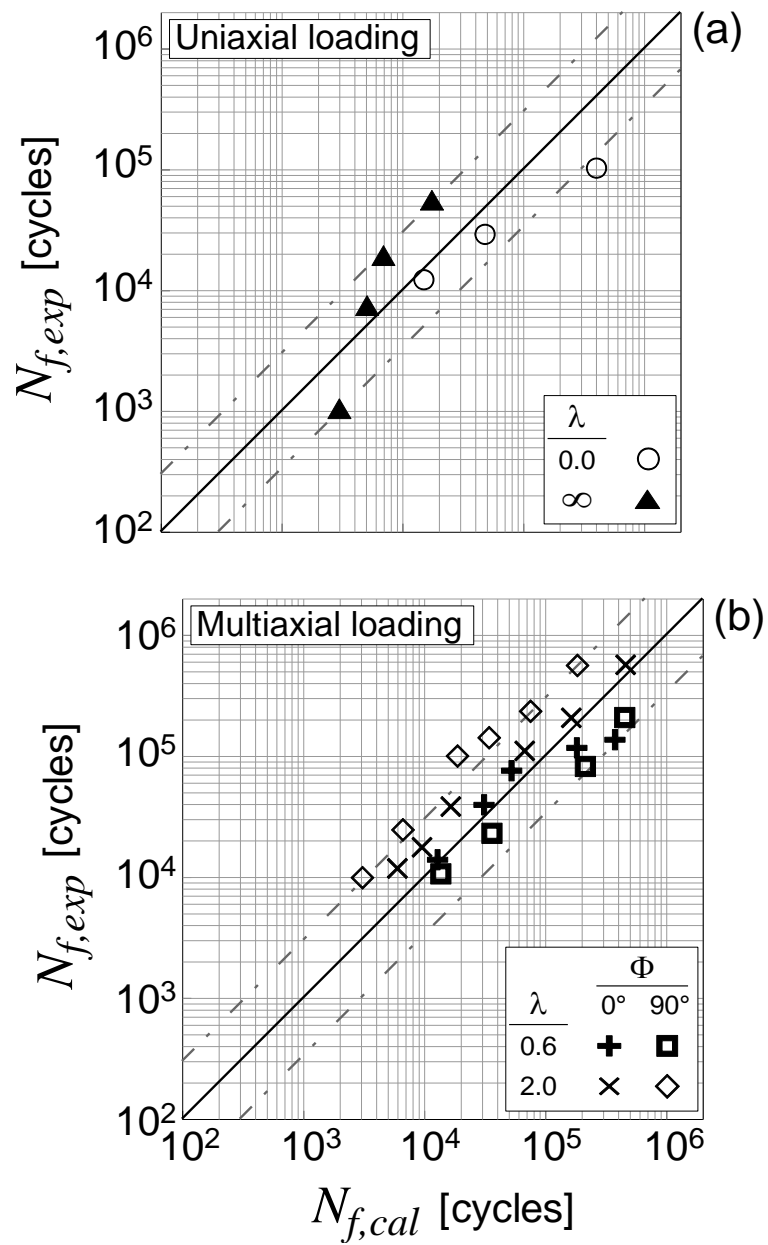
Figure 6. Comparison between theoretical and experimental fatigue life: (a) uniaxial loading; (b) multiaxial loading.
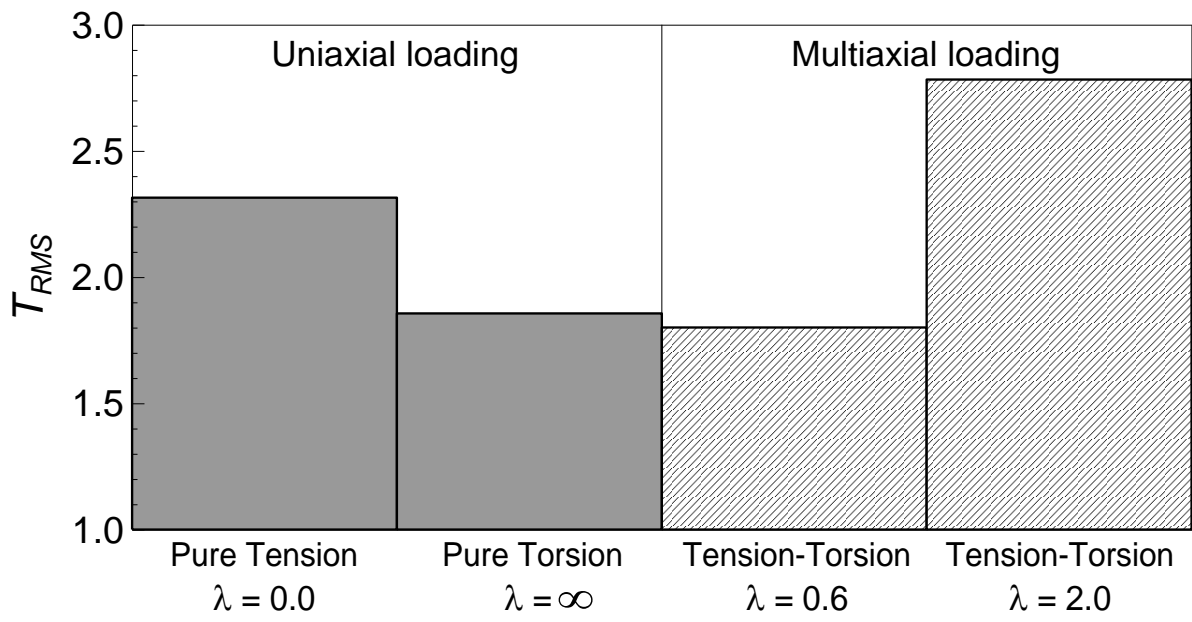
Figure 7. Mean square error determined by applying the strain-based criterion together with the control volume concept, for different loading conditions.